Mixing Behavior of Alkoxylated Dehydrobenzo[12]annulenes at the Solid–Liquid Interface: Scanning Tunneling Microscopy and Monte Carlo Simulations

Shengbin Lei,[†,§,*] Kazukuni Tahara,[‡] Klaus Müllen,[∥] Paweł Szabelski,[⊥,*] Yoshito Tobe,[‡,*] and Steven De Feyter[†,*]

[†]Division of Molecular and Nanomaterials, Department of Chemistry and Institute of Nanoscale Physics and Chemistry, Katholieke Universiteit Leuven, Celestijnenlaan 200F, 3001 Leuven, Belgium, [‡]Division of Frontier Materials Science, Graduate School of Engineering Science, Osaka University, Toyonaka, Osaka 560-8531, Japan, [§]Key Laboratory of Microsystems and Microstructures Manufacturing, Ministry of Education & The Academy of Fundamental and Interdisciplinary Science, Harbin Institute of Technology, Harbin 150080, People's Republic of China, [⊥]Department of Theoretical Chemistry, Maria-Curie Skłodowska University, Pl. M.C. Skłodowskiej 3, 20-031 Lublin, Poland, and [∥]Max Planck Institute for Polymer Research, Ackermannweg 10, 55128 Mainz, Germany

ABSTRACT We present a systematic scanning tunneling microscopic study on the mixing behavior of molecules (DBAs) with different alkyl substituents at the solid–liquid interface to reveal the phase behavior of complex systems. The phase behavior of binary mixtures of alkylated DBAs at the solid–liquid interface can be predicted by the 2D isomorphism coefficient. In addition, we also investigated the influence of coadsorption of template molecules on the phase behavior of DBA mixtures. Coadsorption of these molecules significantly promotes mixing of DBAs, possibly by affecting the recognition between alkyl chains. Monte Carlo simulations prove that the 2D isomorphism coefficient can predict the phase behavior at the interface. These results are helpful for the understanding of phase behavior of complex assembling systems and also for the design of programmable porous networks and hierarchical architectures at the solid–liquid interface.

KEYWORDS: self-assembly · scanning tunneling microscopy · physisorption · phase behavior · multicomponent

The self-assembly of nanometer-sized building blocks on surfaces and at interfaces is a powerful way to fabricate complex molecular nanostructures following the bottom-up principle.[1−12] Surface-confined two-dimensional (2D) molecular networks, especially those with void spaces, so-called "2D porous networks", attract a lot of interest.[1−3,13] These 2D porous networks are used as hosts to immobilize functional units as guest molecules in a repetitive and spatially ordered arrangement and also as a platform for the construction of molecular devices.[14−19] The porous networks are typically sustained *via* hydrogen bonds, metal–ligand coordination, or even van der Waals interactions. The size and geometry of the pores, actually nanowells, in the networks could be easily tailored by adjusting the size and symmetry of the building blocks[20−23] as well as the substrate.[24] Functionalization of these networks was achieved by introducing functional groups to the building blocks.[25,26] Among them, the networks formed by alkoxylated dehydrobenzo[12]annulenes (DBAs) *via* alkyl chain interdigitation represent an interesting case.[27−31] The flexibility of the alkyl chains and the weak van der Waals interactions between them make the supramolecular network quite flexible. These networks were observed to change their structure not only in response to the inclusion of "static" guest molecules but also in response to the dynamics of clusters of guest molecules captured in the nanowells.[31]

Molecular recognition at interfaces involves many simultaneous interactions based on molecular shape, size, functional groups, *etc.*[32−37] The weak thus reversible supramolecular interactions sustaining these networks enable the system to exhibit a substantial degree of dynamic behavior and self-repair, which is a prerequisite for the readout of structural and functional information stored in the building blocks and for obtaining highly ordered and defect-poor assemblies.[38,39]

The mixing behavior of molecules upon adsorption from solution to the interface is central for many phenomena of industrial and academic relevance. Therefore, understanding

* Address correspondence to leisb@hit.edu.cn, szabla@vega.umcs.lublin.pl, tobe@chem.es.osaka-u.ac.jp, steven.defeyter@chem.kuleuven.be.

Received for review March 6, 2011 and accepted April 18, 2011.

Published online April 18, 2011
10.1021/nn200874k

the fundamental aspects controlling the phase behavior of molecular mixtures at an interface is of particular importance. The adsorption of a binary mixture of two species with similar structure represents an ideal, simplified model system. Clarke and co-workers have investigated the mixing behavior of linear alkanes and alkane derivatives (alcohols and acids) in "solid" monolayers at the liquid−solid interface using calorimetry and incoherent elastic neutron scattering (IOENS).[40−42] For these compounds, which carried the same functional group but differed in chain length, a clear dependence of the mixing behavior on the difference of chain length was detected: a large chain length difference leads to complete phase separation, while mixing is promoted upon decreasing the difference in chain length. A quantitative parameter, the 2D isomorphism coefficient, which is defined as $I_{2D} = 1 - A_{un}/A_{com}$, where A_{un} and A_{com} are the areas uncommon and common for the unit cells of both species, was used to predict the extent of mixing in binary monolayers.[43]

The interactions between interdigitated alkyl chains in the DBA networks are quite similar in nature to those of linear alkanes or alkane derivatives. However, in the case of linear alkanes, changing the alkyl chain length only affects the unit cell vector in one direction, while in a truly 2D network of DBAs, it affects both unit cell vectors. From the viewpoint of designing functional nanosystems,[44−47] the porosity of these networks and their capability to accommodate guest molecules make DBA systems highly appealing.

Computational approaches have been a complementary way to study the self-assembly of functional molecules on solid surfaces. A modeling input enables us not only to understand the key factors affecting the assembly at the microscopic scale but also to predict the morphology of thermodynamically stable phases. The most popular methods to model the formation and structure of 2D molecular networks have been molecular dynamics (MD)[48] and density functional theory (DFT),[49−53] though only small assemblies can be treated. Another, somewhat underestimated, simulation technique in the field of 2D self-assembly is the Monte Carlo (MC) method which offers the possibility of investigating large molecular systems under variable conditions.[54,55] An important merit of this technique is that it can mimic the spontaneous self-organization of functional molecules into naturally emerging 2D patterns without imposing any constraints on the symmetry of the final superstructure.[56] Furthermore, the MC method is able to reproduce the coexistence of different phases and to predict conditions under which these phases are stable. The robustness of the MC method is particularly visible in lattice models in which the substrate and adsorbed molecules are represented in a simplified way.[57] Even though the MC method seems ideally suited for modeling 2D supramolecular architectures, its practical use has been reported for a rather limited number of experimental systems.[58−60]

In this study, we investigated the phase behavior of binary mixtures of DBAs with alkoxy chains of different length at the solid−liquid interface, by means of both STM and theoretical simulations using the Monte Carlo method. By this investigation, we show that (1) STM is able to characterize the mixing behavior of such systems with high spatial resolution and sensitivity; (2) these more complex 2D networks follow similar rules as developed from the linear alkane and alkane derivatives; that is, an increased tendency of phase separation was observed with increased difference in alkoxy chain length; (3) the porosity of the networks is maintained upon mixing; (4) the accommodation of template or guest molecules significantly influences the mixing behavior of DBAs in the monolayer; (5) by mixing DBAs with different alkoxy chain length, the symmetry of the networks as well as the number of templates or guests per cavity can be tuned; and (6) the phase behavior of these DBAs can be reproduced using Monte Carlo simulations.

RESULT AND DISCUSSION

Assembling Behavior of DBA Binary Mixtures. As reported previously,[61] the self-assembly structure formed by these DBAs at the TCB/graphite interface depends sensitively on the concentration. This turns out to be true also for the binary mixtures of DBAs with different alkoxy chains. One example is shown in Figure 1 (see also Figures S1 and S7 in Supporting Information). DBA-OC_{10} forms always honeycomb networks irrespective of its concentration when coadsorbed with DBA-OC_{20}. DBA-OC_{20} forms either a nonporous linear pattern or a porous honeycomb structure, depending on its concentration. Always phase separation was observed due to the large difference in alkoxy chain length. The surface coverage of the individual species though depends on the concentration.[62]

To simplify the analysis, all experiments of binary DBA mixtures at the TCB/graphite interface were carried out at a concentration[63] where both species form dominantly porous honeycomb networks. We have investigated different combinations of DBAs with variable alkoxy chain length difference: two, four, six, and even more methylene groups.

For binary mixtures of DBAs which differ in the alkoxy chain length by two methylene units, two pairs are investigated: DBA-OC_{14}/DBA-OC_{16} and DBA-OC_{16}/DBA-OC_{18}. Typical STM images of monolayers formed by the DBA-OC_{14}/DBA-OC_{16} binary mixture are shown in Figure 2. On a large scale, phase separation is revealed with pure domains of DBA-OC_{14} and DBA-OC_{16} (Figure 2a). At this concentration (DBA-OC_{14} = 3.2×10^{-6} M, DBA-OC_{16} = 2.9×10^{-6} M), DBA-OC_{14} predominately forms porous honeycomb networks,

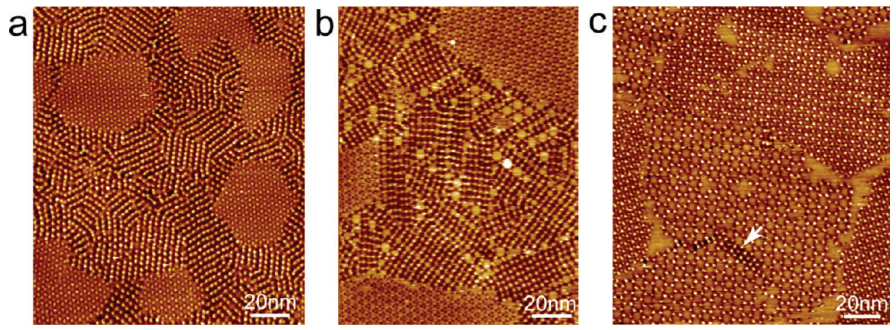

Figure 1. Assemblies formed by a binary mixture of DBA-OC_{10} and DBA-OC_{20} at different concentrations. (a) DBA-OC_{10} = 2.0 × 10^{-5} M, DBA-OC_{20} = 1.2 × 10^{-5} M; (b) DBA-OC_{10} = 2.0 × 10^{-6} M, DBA-OC_{20} = 1.2 × 10^{-6} M; (c) DBA-OC_{10} = 8.1 × 10^{-7} M, DBA-OC_{20} = 4.8 × 10^{-7} M. In (a), DBA-OC_{20} exists exclusively as linear structure. In (b), DBA-OC_{20} forms dominantly linear structure, but a small portion of honeycomb structure also exists, while in (c), DBA-OC_{20} forms predominantly honeycomb structure with only a small portion of linear structure (marked by the white arrow).

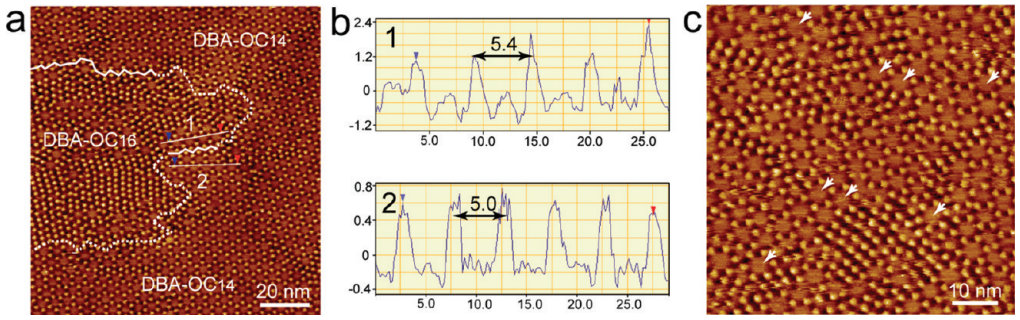

Figure 2. STM image showing phase separation of DBA-OC_{14} and DBA-OC_{16} at the TCB/graphite interface (a). The section profiles corresponding to the lines marked in the image are shown in (b). The 5.4 nm periodicity measured in line 1 indicates a DBA-OC_{16} network, while the 5.0 nm periodicity in line 2 is characteristic of a DBA-OC_{14} network. Note that domain boundaries could be identified with molecular accuracy in some areas, as shown in (a) with the solid white lines. In other areas, domain boundaries could be defined only roughly (dotted lines) due to mixing of both molecules. In some areas (c), these two molecules show pronounced mixing, and no clear boundaries could be identified. The white arrows highlight some of the larger cavities, which are formed by mainly or only DBA-OC_{16}. Concentration DBA-OC_{14} = 3.2 × 10^{-6} M, DBA-OC_{16} = 2.9 × 10^{-6} M.

while for DBA-OC_{16}, honeycomb networks coexist with nonporous linear patterns. As shown in Figure 2b, DBA-OC_{14} and DBA-OC_{16} domains could be identified by measuring the periodicity of the networks. However, a pronounced fraction of nano- and molecular scale mixing was also observed in some areas (Figure 2c), where hybrid honeycomb networks formed by DBA-OC_{14} and DBA-OC_{16} are revealed to coexist with pure DBA-OC_{14} and DBA-OC_{16} networks (some of the honeycombs formed by DBA-OC_{16} are indicated with white arrows in Figure 2c). Hybrid networks are characterized by a slight distortion in symmetry, irregular size, and periodicity. The existence of hybrid networks also makes it difficult to identify the domain boundaries. It is worth noting that, though there is a about 0.5 nm difference in the repeating period between the networks formed by DBA-OC_{14} and DBA-OC_{16}, it is not straightforward to distinguish between both networks in the STM images, especially in large-scale images. This makes it difficult to exactly quantify the extent of phase separation by analyzing the surface coverage of individual networks.

For mixtures of DBA-OC_{16} and DBA-OC_{18}, it is even harder to identify the DBAs and to evaluate the phase behavior (see Figure S2 in Supporting Information). An increased mixing is anticipated.

As the alkoxy chain length difference increases to four methylene groups, like DBA-OC_{14}/DBA-OC_{18}, a more pronounced phase separation is revealed (Figure 3a). Due to the increased difference in unit cell parameters, now honeycomb networks of pure DBA-OC_{14} and DBA-OC_{18} could be distinguished clearly. However, thanks to the high spatial resolution of STM, at domain boundaries, some extent of mixing was still observable, as shown in Figure 3b. In the center of this image, some hybrid networks can be seen, with the aromatic core of DBA-OC_{14} and DBA-OC_{18} highlighted with yellow and blue circles, respectively. Some nanometer-sized DBA-OC_{14} domains could also be observed in the center of a DBA-OC_{18} domain and *vice versa*.

For binary mixtures of DBAs with an even larger difference in alkoxy chain length (six methylene units and above), complete phase separation was revealed, without mixing even at domain boundaries (Figure 1 and Figure 4).

For linear alkane and alkane derivatives, the mixing behavior in the adsorbed layers at the liquid–solid interface depends upon both the symmetry and the

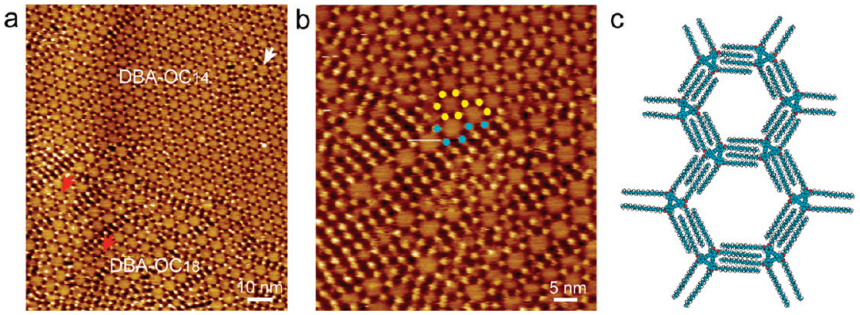

Figure 3. Large-scale (a) and smaller-scale (b) STM images of the monolayer formed by a binary mixture of DBA-OC_{14} and DBA-OC_{18}. Pronounced phase separation is observed in general. Nanometer-sized DBA-OC_{18} (DBA-OC_{14}) domains surrounded by DBA-OC_{14} (DBA-OC_{18}) domains are highlighted by white (red) arrows. In (b), hybrid networks are observed at domain boundaries, and the aromatic cores of DBA-OC_{14} and DBA-OC_{18} are highlighted with yellow and blue circles. A tentative model of the hybrid network is shown in (c). Concentration DBA-OC_{14} = 3.2 × 10^{-6} M, DBA-OC_{18} = 5.2 × 10^{-7} M.

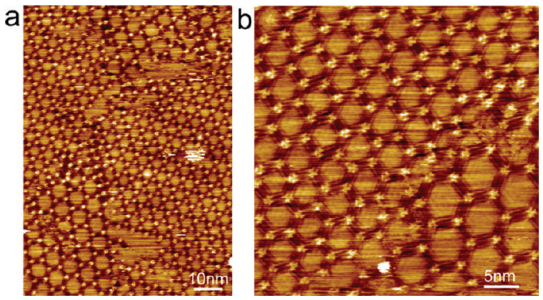

Figure 4. STM images revealing the phase separation in a monolayer of DBA-OC_{14} and DBA-OC_{20} at the TCB/graphite interface. Concentration DBA-OC_{14} = 1.6 × 10^{-6} M, DBA-OC_{20} = 1.2 × 10^{-6} M.

quantitative similarity of the unit cells of the two pure monolayers. To express quantitatively the similarity of the unit cells of two alkane derivatives, Clarke *et al.* proposed a parameter, the 2D isomorphism coefficient I_{2D},[64] which is defined as $I_{2D} = 1 - A_{un}/A_{com}$, where A_{un} and A_{com} are the areas uncommon and common for the unit cells of both species. This parameter is analogous to the isomorphism coefficient used to define the unit cell similarity of alkanes. It explains the bulk phase behavior of alkane mixtures, being defined in terms of areas instead of volumes.[65] Though several other parameters and models were also proposed to describe the mixing behavior of binary mixtures like alkanes,[66] surfactant,[67] and lipids,[68] we chose the 2D isomorphism coefficient due to its simplicity and high relevance to the current system. The 2D isomorphism coefficient of the binary mixtures tested in the above experiments and their corresponding phase behavior at the interface are summarized in Table 1. For the binary mixtures with components differing in the alkoxy chain length by only two methylene groups, the value of I_{2D} falls in the range of 0.82 and above, and significant mixing was revealed. For the combinations with alkoxy chains differing by four methylene groups, only a small extent of mixing was detected at domain boundaries. For combinations with an even larger difference in alkoxy chain length, complete phase separation was revealed, without mixing even at domain boundaries. The I_{2D} values for these combinations are smaller than 0.7. Noteworthy, the I_{2D} value for the combination DBA-OC_{10}/DBA-OC_{20} even shows a negative value due to the big difference of the unit cells. Though we have difficulties unequivocally identifying DBA molecules with very similar alkoxy chains (difference of only two methylene groups), especially in large-scale STM images, a qualitatively similar trend as revealed for alkane/alkane derivatives is observed: complete phase separation happens for small I_{2D} values, while with an increasing isomorphism coefficient, partial mixing to complete mixing is expected. The onset of partial mixing for alkanes and alcohols was found to be around I_{2D} = 0.7, and ideal mixing happens when I_{2D} reaches 0.9.[64] For the DBA networks, the I_{2D} value for the onset of partial mixing is expected to lie between 0.61 and 0.82 (Table 1).

TABLE 1. Summary of the Phase Behavior of Binary Mixtures in the Absence and Presence of Template Molecules

			phase behavior	
combination	chain length difference[a]	I_{2D}[b]	without template	with template
DBA-OC_{18}/DBA-OC_{20}	2	0.86	NA	mixing
DBA-OC_{16}/DBA-OC_{18}	2	0.84	mixing	NA
DBA-OC_{14}/DBA-OC_{16}	2	0.82	partial mixing	mixing
DBA-OC_{16}/DBA-OC_{20}	4	0.66	NA	partial mixing
DBA-OC_{14}/DBA-OC_{18}	4	0.61	phase separation	partial mixing
DBA-OC_{14}/DBA-OC_{20}	6	0.42	phase separation	partial mixing
DBA-OC_{10}/DBA-OC_{20}	10	−0.36	phase separation	phase separation

[a] Expressed in number of methylene groups. NA: not assigned. [b] I_{2D} was calculated according to the unit cell parameters of the honeycomb network of DBAs; to differentiate from I_{2Dt}, we call it experimental 2D isomorphism coefficient.

Monte Carlo Simulation. To gain further insight in the phase behavior, theoretical simulations with lattice

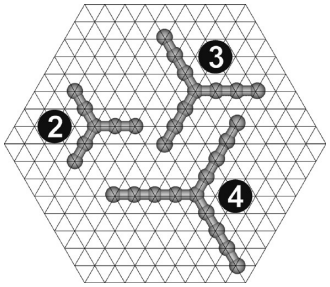

Figure 5. Examples of molecular structures used in the Monte Carlo simulations. The tripods consist of a central segment (core) and three arms composed of *n* segments each. The numbers in the figure, *n*, refer to the arm length of the corresponding molecule.

Monte Carlo method were conducted. In order to simulate the mixing behavior of the binary mixtures, we first built a simple and general model that is able to reproduce the common honeycomb structure of ordered monolayers formed by chemically different tripod-shaped organic molecules. The construction of the model and simulation on the single-component system was reported in detail elsewhere.[55] In our model, as a first approximation, we neglect system-dependent factors such as flexibility of the molecular building block, influence of solvent, and the possibility of desorption of the molecules from the surface.

The DBA molecules were represented by flat rigid structures composed of a central segment called "core" with three *n*-membered arms attached to it, as shown schematically in Figure 5. Accordingly, a molecule of size *n* comprised $3n + 1$ segments, each of which was allowed to occupy one adsorption site, which is one vertex of the lattice. In the simulation, the mixture always consisted of equal numbers (100 + 100) of molecules differing by one or two segments per arm. The simulations were performed on a simple triangular $L \times L$ lattice of adsorption sites using the conventional canonical Monte Carlo method with Metropolis sampling.[69] In addition to the standard MC moves, including translation and rotation of a molecule, we also used swap moves (exchange of unlike molecules) whose attempt frequency was set to 20%. Specifically, a single swap move involves a random selection of a pair of unlike molecules followed by an attempt to exchange their identities. To that purpose, the arms of the small molecule are each elongated by a desired number of segments (here by 1 and 2), and the arms of the big molecule are simultaneously shortened by the same number of segments. The original positions and orientations of both molecules remain unchanged. Next, potential energies of the original and new configuration are compared, and the swap move is accepted using the classical Metropolis acceptance rule.[69] As we observed, including these moves did not change qualitatively the obtained results, as the density of the adsorbed phase considered here was very low and

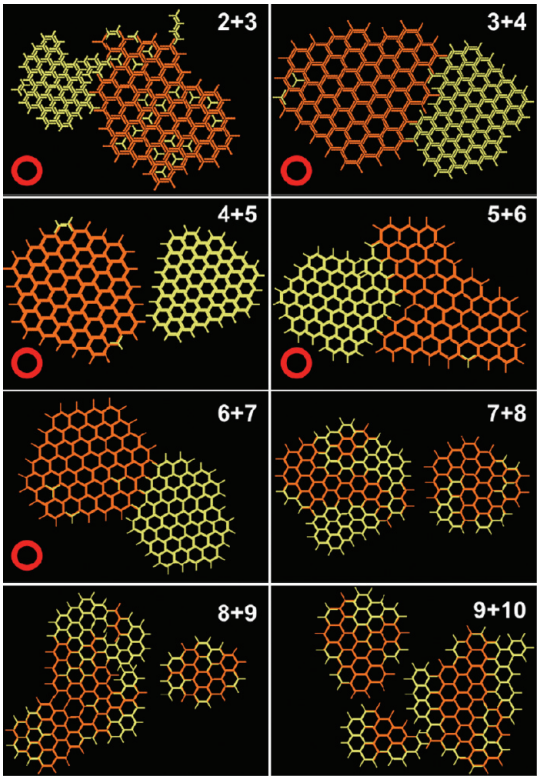

Figure 6. Mixing behavior of tripod molecules differing by one segment ($\Delta n = 1$) in an arm (equimolar mixture, scale is not preserved). The white numbers in the upper left corner, $n' + n''$, indicate the number of segments (n) in each arm for each of the components. A red circle in the bottom left corner indicates phase separation.

equilibration of the adlayer occurred quite fast even when the swapping was switched off. To trace pseudotemporal evolution of the system, we used a "time" unit equal to one MC step being a single attempt of changing the system state by means of translating and rotating a molecule or by swapping a pair of molecules.

As mentioned previously,[55] the simulations were carried out assuming low density of the adsorbed phase, ρ, which was defined as the total number of molecular segments adsorbed on the lattice divided by the lattice area, L^2. For molecules differing by one segment per arm, the density was equal to 0.0425, while for the molecules differing by two segments per arm, it was set to 0.05. To keep constant density of the mixed adsorbed phases composed of molecules with different *n*, the lattice size was appropriately rescaled (see Supporting Information and Table S1). Interactions between molecules were restricted to nearest neighboring segments on a triangular lattice. The energy of interaction between a molecular core and an arm segment was characterized by ε_c and that between two arm segments by ε_a. Both energy terms are expressed in kT units.

Our previous simulations on single-component systems indicate that the formation of honeycomb networks depends both on the length of the arm

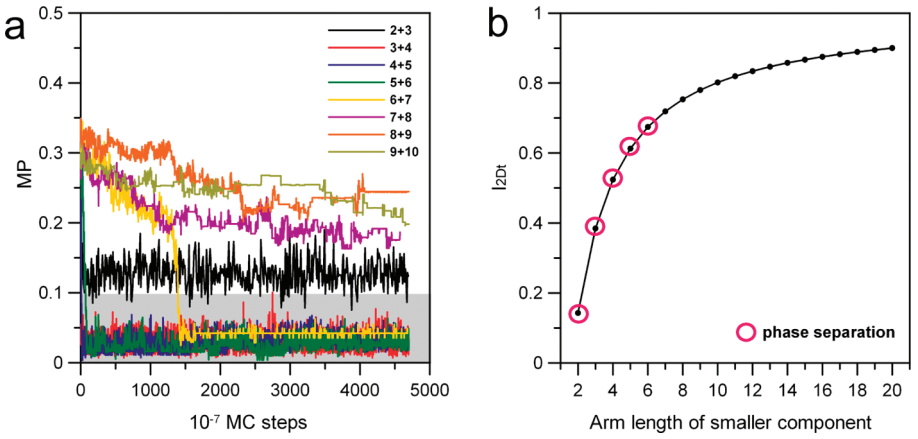

Figure 7. (a) Temporal evolution of MP, the number of heterogeneous interactions per segment, for equimolar binary mixtures of molecules differing by one segment in an arm, *i.e.*, $\Delta n = 1$ and (b) I_{2Dt}: theoretical 2D isomorphism coefficient of different mixtures. The red circles mark the mixtures in which phase separation was observed.

Chart 1. Chemical structures of the DBAs (left) and nanographene (right) molecules.

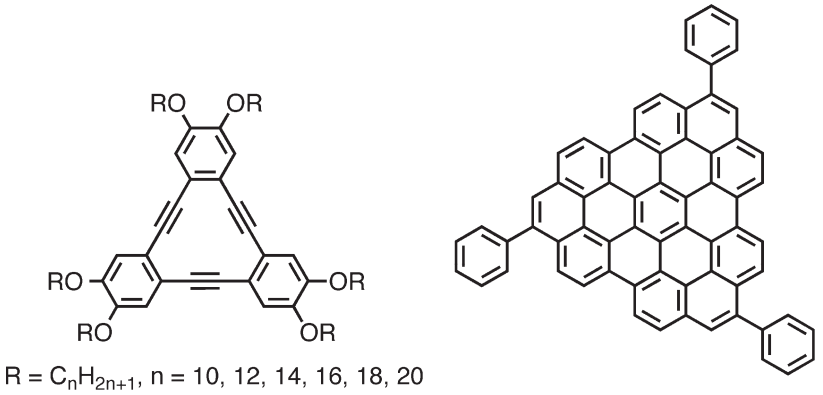

segments and the properties of the core segment.[55] For example, in case of $\varepsilon_c = \varepsilon_a$, which means that interactions between core−arm and arm−arm segments are identical and attractive, the molecules form exclusively honeycomb networks when $n \geq 2$. In contrast, when a repulsive interaction between core and arm segments was assumed, completely different patterns could be formed. For this reason, in the simulation of binary mixtures, we assumed that the molecules are composed of identical segments, that is, $\varepsilon_c = \varepsilon_a = 1\ kT$. As we examined, this value guarantees also the formation of the honeycomb pattern at the densities considered here, regardless of $n \geq 2$. Note that in the approach adopted here there is no direct correspondence between a segment and a chemical building block of a real molecule. Thus, this is a simple but general model for the assembly of tripod-shaped molecules.

Figure 6 shows snapshots of MC simulations of a layer from an equal mole mixture of $n = n'$ and $n = n'' = n' + 1$ molecules (*i.e.*, $\Delta n = 1$). The snapshots marked with red circles indicate immiscibility of the components. The simulations show that segregation occurs for $n < 6$. Interestingly, in the case $2 + 3$ (*i.e.*, $n' = 2$ and $n'' = 3$), smaller molecules are "coadsorbed" in the hexagons formed by the bigger molecules. For the $\Delta n = 2$ mixtures, analogous results were obtained (see Figure S10 in Supporting Information): segregation occurs for $n < 11$. A notable characteristic of mixing is the distortion of honeycomb networks (lower part of Figure 6). The same phenomena were also observed in the assembling of DBAs (DBA-OC_{14}/DBA-OC_{16}, for instance, as shown in Figure 2). Thus, though it is difficult to distinguish different DBAs in the STM images due to the similarity in structure and size, the increase in network distortion could serve as an indication of mixing.

A problem is how to define whether and to what extent the components mix in the modeled system. Here we proposed a parameter which is informative at least in a qualitative way. The mixing parameter (MP) is the number of heterogeneous interactions per molecular segment in the mixture. More precisely, it is the number of neighboring pairs of segments belonging to unlike molecules divided by the total number of segments in the system. If it is 0, a complete separation without even phase boundary occurs. Thus, the extent of separation can be measured using this parameter and inspected visually.

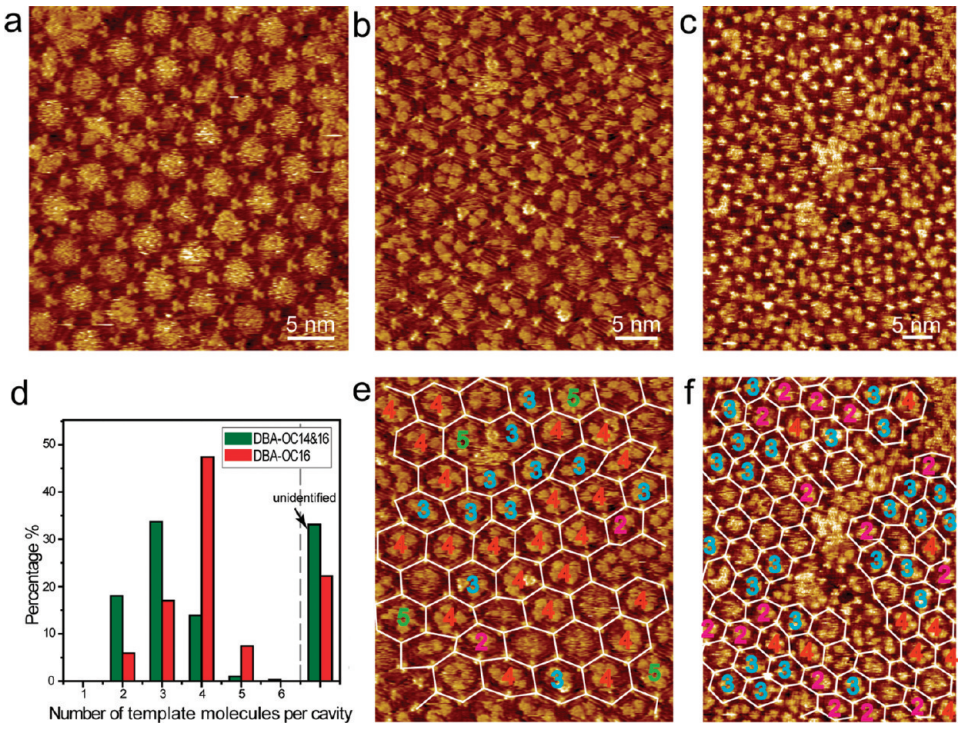

Figure 8. Comparison of the host–guest architectures formed by DBA-OC_{14} (a), DBA-OC_{16} (b), and a mixture of DBA-OC_{14} and DBA-OC_{16} (c) with nanographene 1. Panels e and f are identical to panels b and c, respectively: however, the host network is highlighted with white lines to guide the eye, and the number of template molecules in each cavity is marked with characters of different color. A histogram of the distribution of the number of template molecules per cavity (n_t) in the pure DBA-OC_{16} network (red) and mixed network (green) is shown in (d). In the histogram, the last column represents the population of cavities with an unidentified number of template molecules. Concentration DBA-OC_{14} = 1.6 × 10^{-5} M, DBA-OC_{16} = 1.4 × 10^{-5} M, nanographene = 2.1 × 10^{-6} M.

Figure 7a plots MP as a function of the number of the MC steps calculated for the $\Delta n = 1$ mixture, for different values of n. As it is seen in the figure, MP drops sharply below 0.1 for n lower than 7, indicating immiscibility of the components. Obviously, the exception is the case 2 + 3 for which the higher value of MP corresponds to the inclusion effect mentioned above. Thus, visual inspection of the layer is always needed. Note that these results agree fully with what is seen in the snapshots from Figure 6. We got similar results for $\Delta n = 2$ systems, and the mixing occurs for $n < 10$ (Figure S11 in Supporting Information).

To compare the results from simulation with those obtained from the experiments, we calculated the theoretical 2D isomorphism coefficient (I_{2Dt}, see Supporting Information) of the different mixtures simulated (Figure 7b). The data points that correspond to systems with immiscible components are highlighted with red circles. For $\Delta n = 1$, a threshold value around 0.7 was found, which is in good agreement with the experimental observations.

Effect of Template Inclusion. An interesting aspect of 2D nanoporous networks is its "host–guest" behavior.[1,13] As stated previously, the DBA networks are sustained by van der Waals interactions between interdigitated alkyl chains. The recognition between alkyl chains of the same length in order to maximize the interdigitation energy plays an important role in governing the phase behavior of a binary mixture of DBAs. When template or guest molecules are part of the monolayer, the interactions between these molecules

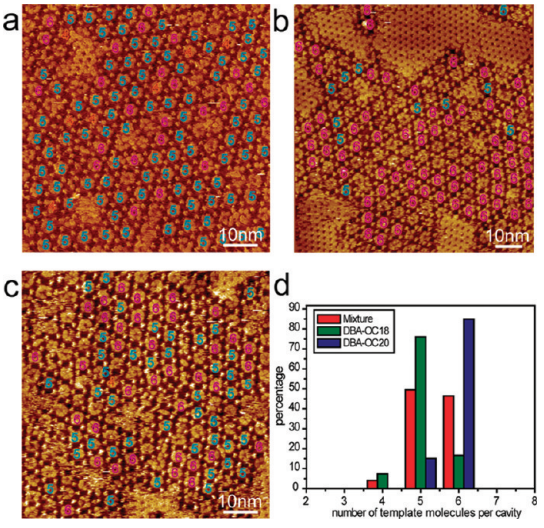

Figure 9. STM images of the host–guest architecture of DBA-OC_{18} (a), DBA-OC_{20} (b), and a mixture of DBA-OC_{18} and DBA-OC_{20}. The number of nanographene templates is marked on the images with different colors, and the distribution of n_t is shown in (d). Concentration DBA-OC_{18} = 1.3 × 10^{-5} M, DBA-OC_{20} = 1.2 × 10^{-5} M, nanographene = 2.1 × 10^{-6} M.

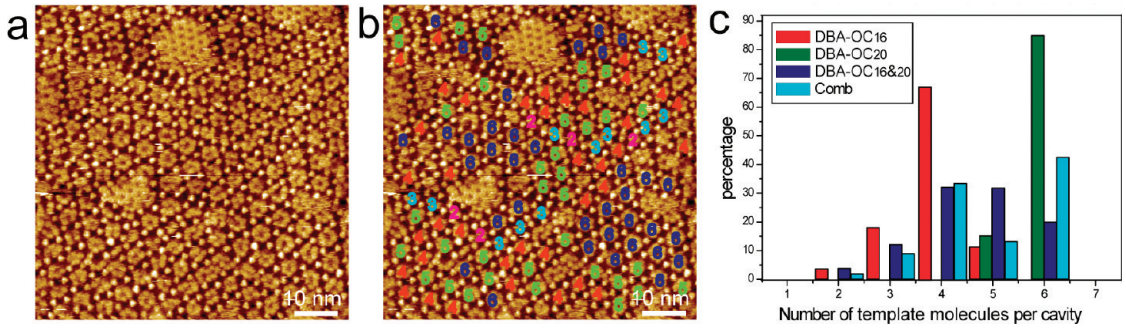

Figure 10. (a) Hybrid network formed by the mixture of DBA-OC_{16} and DBA-OC_{20} at the TCB/graphite interface in the presence of nanographene; (b) is identical to (a). In (b), the number of nanographenes in each cavity is marked with different colored characters. The distribution of n_t in both pure DBA-OC_{16} and DBA-OC_{16}/DBA-OC_{20} networks is shown in (c). Concentration DBA-OC_{16} = 1.4 × 10^{-5} M, DBA-OC_{20} = 1.2 × 10^{-5} M, nanographene = 2.1 × 10^{-6} M.

and host network could interfere with the above-mentioned recognition process and thus influence the phase behavior of the DBAs.

In the following experiments, we investigated the influence of template or guest inclusion on the phase behavior of DBA mixtures. To do so, a strategy which was called "*structural transformation by inclusion of a template*" was used.[30,31] In this case, the DBAs do *not* form intrinsically porous networks at the concentration used. Instead, the formation of porous networks is induced by template molecules.

As reported previously,[31] nanographene **1** (the structure is shown in Chart 1) could efficiently induce such a structural transformation for certain alkoxylated DBAs, namely, from a template-free close-packed linear pattern to a template-filled porous honeycomb pattern, with one to six nanographenes accommodated in each cavity, depending on the length of the alkoxy chains. However, due to the flexibility of the DBA networks, there is a distribution of the number of template molecules per pore (Figures 8 and 9). Nevertheless, there always exists a most abundant, characteristic nanographene cluster for each DBA, such as a tetramer for DBA-OC_{16} (see also Figure S3 in Supporting Information), a pentamer for DBA-OC_{18}, and a hexamer for DBA-OC_{20}. When two different DBAs coexist at the interface, the spatial distribution of these characteristic clusters could be used as an indication of phase separation.

Figure 8 shows a comparison of the host–guest architecture formed by nanographene **1** with pure and mixed DBA networks (see also Figure S4 in Supporting Information). In the architecture formed by DBA-OC_{14} and nanographene **1**, the nanographene molecules in the cavities are mobile. This leads to a time-averaged interaction with the edges of the hexagon cavity, and therefore, the networks appear almost intact with good symmetry. This is similar to the case of porous networks formed under concentration control in the absence of template, where the porous networks are thought to be stabilized by the coadsorption of laterally mobile solvent molecules. In contrast, for DBA-OC_{16}, in most cavities, the template molecules are fixed by the spatial constraints and the network is more distorted (see Figure 8e). As shown in Figure 8d, the histogram of the number of template molecules per cavity (n_t) in the DBA-OC_{16} network shows a distribution between 2 and 6. Tetramers (n_t = 4) are the most abundant clusters. This distribution was considered to be an indication and the result of the flexibility of the DBA network. Therefore, the distribution of n_t can be used as an indication of mixing for bicomponent DBA systems. As shown in Figure 8d, upon mixing of DBA-OC_{14} and DBA-OC_{16} in the presence of the nanographene template, a remarkable change is the significantly increased abundance of immobilized nanographene dimers and trimers. As the number of templates per cavity (n_t) can not be identified in the DBA-OC_{14} network,[31] while tetramers are the most abundant species in the DBA-OC_{16} network, the increased abundance of dimers and trimers in the mixed binary network is an indication of the formation of hybrid networks by both DBAs. The hybrid network is expected to possess smaller cavities in comparison with that of DBA-OC_{16}. Another difference is the increased population of cavities with fuzzy features (corresponding to the unmarked cavities in Figure 8e,f and indicated in the histogram (Figure 8d) as "unidentified") with respect to DBA-OC_{16}. These could be partially attributed to networks formed by pure DBA-OC_{14}.

In addition, the spatial distribution of characteristic clusters can serve as an indication of phase separation of the corresponding DBAs. For instance, the spatial distribution of the clusters in the mixed network (Figure 8f) shows no significant local enrichment of tetramers—the characteristic host–guest architectures formed by pure DBA-OC_{16} and nanographene (Figure 8e)—and confirms good compatibility of DBA-OC_{14} and DBA-OC_{16} in the assembly.

For the combination DBA-OC_{18} and DBA-OC_{20} with higher I_{2D}, the histogram (Figure 9) indicates a nearly equal abundance of pentamers and hexamers, which implies there is no significant preferential adsorption (see also Figures S5 and S6 in Supporting Information).

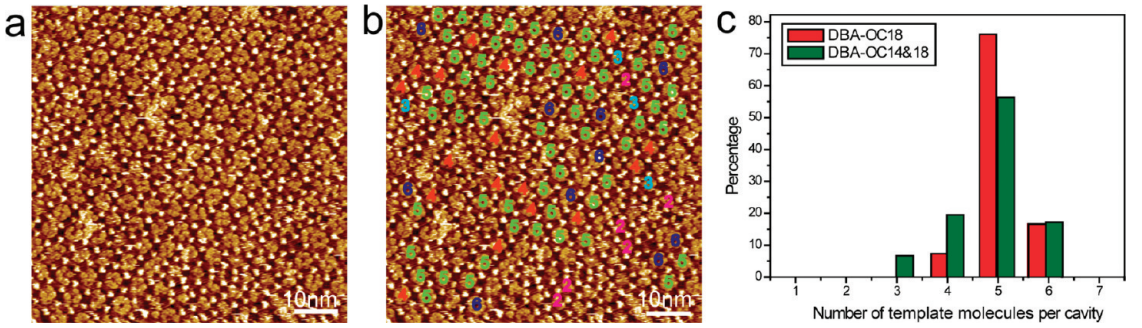

Figure 11. (a) Hybrid network formed by the mixture of DBA-OC_{14} and DBA-OC_{18} at the TCB/graphite interface in the presence of nanographenes; (b) is identical to (a). In (b), the number of nanographenes in each cavity is marked with different colored characters. The distribution of n_t in both pure DBA-OC_{18} and DBA-OC_{14}/DBA-OC_{18} networks is shown in (c). Concentration DBA-OC_{14} = 1.6 × 10^{-5} M, DBA-OC_{18} = 1.3 × 10^{-5} M, nanographene = 2.1 × 10^{-6} M.

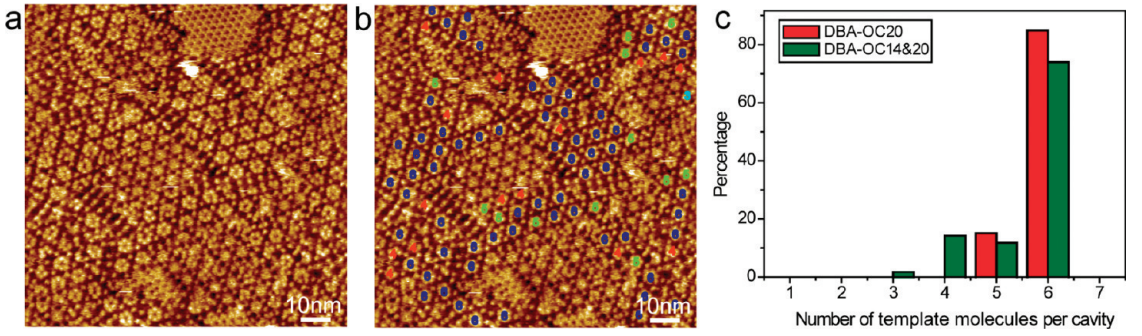

Figure 12. STM images (a,b) and histogram of distribution of n_t in the network (c) formed by mixture of DBA-OC_{14}/DBA-OC_{20}. Concentration DBA-OC_{14} = 1.59 × 10^{-5} M, DBA-OC_{20} = 1.20 × 10^{-5} M, nanographene = 2.10 × 10^{-6} M. Panel b is identical to panel a. The number of nanographenes in each cavity is marked with different colored characters.

Again the spatial distribution of the characteristic clusters (Figure 9c) could be used to evaluate the degree of mixing. In pure DBA-OC_{18} and DBA-OC_{20} networks, pentamers and hexamers are the typical nanographene clusters, respectively. In the bicomponent network, these clusters are distributed nearly randomly, which indicates that the two DBAs are probably mixed ideally in the monolayer.

With an increased difference in alkoxy chain length, the spatial distribution of template clusters in the mixed network of DBA-OC_{16}/DBA-OC_{20} (four methylene difference) indicates a significant tendency of phase separation, which shows up as a nonrandom distribution of nanographene hexamers and smaller clusters in different areas, as shown in Figure 10b. However, the phase separation is not complete, as revealed in the histogram shown in Figure 10c. The distribution of n_t in the mixed network (dark blue) clearly shows an increased abundance of pentamers in comparison with the distribution expected for a complete phase separation without preferential adsorption (light blue).[70] Simultaneously, the histogram also indicates a significant decrease for the abundance of hexamers. On the contrary, the abundance of smaller clusters (dimer to tetramer) shows good agreement with expectation. This change in distribution could be interpreted by a partial mixing of these two DBAs in the presence of nanographene, where the hybrid networks which mainly host pentamers contain more DBA-OC_{20} than DBA-OC_{16}. This could explain why there is a significant decrease in the abundance of hexamers while the abundance of tetramers is nearly not affected. Another possibility is preferential adsorption of DBA-OC_{16}. Though molecules with longer alkyl chains are normally expected to adsorb preferentially due to stronger interaction with the substrate,[71] for the DBAs, this is not necessarily true considering the increased porosity of the network upon elongation of the alkoxy chains. The effect of network porosity on the preferential adsorption of DBAs was reported in detail recently.[62] The coadsorption of the nanographene template could also change the sequence of preferential adsorption. The third possibility is a combination of these factors.

For another combination with a difference in the alkoxy chain length of four methylene groups, DBA-OC_{14}/DBA-OC_{18}, the same trend is revealed as for DBA-OC_{16}/DBA-OC_{20}: partial phase separation happens with a characteristic local enrichment of pentamers and small domains with undistinguishable templates in the cavity. The latter is attributed to DBA-OC_{14} domains and the former to DBA-OC_{18}-rich domains. Though no significant difference could be identified in the spatial distribution of clusters as compared to that in the pure

DBA-OC_{18} network, the histogram of n_t (Figure 11c) reveals a discernible increase in the abundance of tetramers and trimers. Combined with a decrease in the population of pentamers, this could serve as a proof of partial mixing of the two DBAs in the monolayer.

If the difference in alkoxy chain length measures six methylene groups, as for the mixture of DBA-OC_{14} and DBA-OC_{20}, in the presence of nanographene, increased tendency of phase separation is revealed. Surprisingly, the histogram still shows some extent of mixing, that is, an increased abundance of small clusters, which are not frequently observed in pure DBA-OC_{20} networks (Figure 12). Only when the difference in alkyl chain length increased to 10 methylene groups (combination DBA-OC_{10}/DBA-OC_{20}) was the phase separation complete. No significant difference in the distribution of the number of templates per cavity is revealed in comparison with that in pure DBA-OC_{20} and DBA-OC_{10} networks (Figure 13).

Effect of Concentration. Note that the high reversibility of noncovalent interactions involved in the self-assembling of molecules at the solid/liquid interface guarantees the best possible conditions to achieve equilibrium and thus favors the formation of thermodynamically stable structures. However, in some cases, metastable phases could be kinetically trapped and be observed by STM.[13,73]

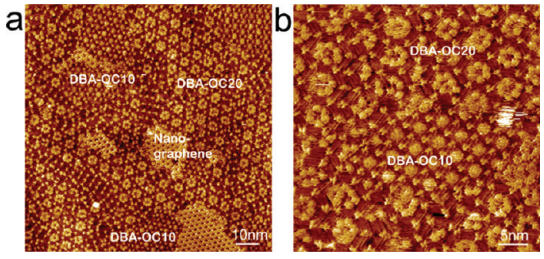

Figure 13. Large-scale (a) and high-resolution (b) STM images show the phase separation of DBA-OC_{10} and DBA-OC_{20} in the presence of nanographene. Concentration DBA-OC_{10} = 2.0 × 10^{-5} M, DBA-OC_{20} = 1.2 × 10^{-5} M, nanographene = 2.1 × 10^{-6} M.

In the "*template inclusion induced transformation*", the honeycomb networks formed by the DBA mixtures presented above are stabilized by the inclusion of nanographenes inside the cavities. Most of these DBAs do not form porous networks intrinsically under these experimental conditions (solvent, concentration) in the absence of template molecules. Upon coadsorption of the template molecules, the networks are more distorted, probably because of unoptimized alkyl chain interdigitation interactions. The question arises if the phase behavior in the presence of the nanographene template represents a kinetically or thermodynamically favored situation. Therefore, the coadsorption of DBA-OC_{14} and DBA-OC_{16} in the presence of nanographene was tested under concentration conditions where both DBAs intrinsically form porous networks. In this case, the nanographene molecules are expected to act as guests. More cavities were characterized with fuzzy features (Figure 14a) in comparison with the networks formed at higher concentration (Figure 8c). A similar observation was made for mixtures of the pure DBA systems and the nanographene template (see Figure S8 in Supporting Information). However, the distribution of n_t only shows a slight shift toward larger clusters: a decrease of dimer and trimers and an increase of tetramers and pentamers. Anyhow, the distribution of n_t is still significantly different from that of pure DBA-OC_{16}. This indicates that the observed stronger tendency toward mixing in the presence of template molecules reflects to a large extent the intrinsic properties of the system, though the mixing behavior in the case of template-induced transformation is indeed affected by kinetic factors.

CONCLUSION

We have investigated the phase behavior of binary mixtures of alkoxylated DBA derivatives which differ in the length of the alkoxy chains, in the absence and presence of a molecular template (*i.e.*, nanographene).

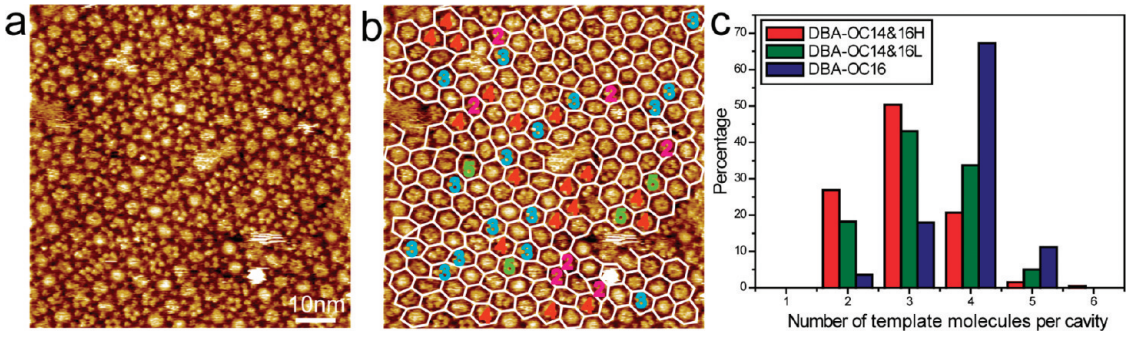

Figure 14. (a) STM image of the host–guest architecture formed by coadsorption of DBA-OC_{14} and DBA-OC_{16} in the presence of nanographene. The concentrations of DBA-OC_{14} and DBA-OC_{16} are 3.2 × 10^{-6} and 2.9 × 10^{-6} M, respectively, while the concentration of nanographene is 2.1 × 10^{-6} M. Panel b is identical to panel a, with the host network highlighted with white lines and the number of template molecules per cavity marked with differently colored characters. The histograms of the distribution of n_t with high (red) and low (green) concentration of DBAs are shown in (c).[72] The histogram of n_t for DBA-OC_{16} (blue) in the absence of DBA-OC_{14} is also shown for comparison.

Table 1 summarizes the phase behavior of the different binary mixtures. In brief, in the absence of nanographene, phase separation is almost complete when the difference in alkoxy chain length reaches four methylene groups. Though the van der Waals interaction between alkoxy chains is relatively weak, it still enables sufficient recognition with reasonable chain length difference. The phase behavior of DBA mixtures could be predicted with the 2D isomorphism coefficient, which was developed by Clarke to predict the phase behavior of simple linear alkanes and alkane derivatives at the liquid–solid interface. To increase our understanding of the mixing behavior at the solid–liquid interface, we also theoretically simulated the mixing process with the lattice gas Monte Carlo method. A simple model reproduces the mixing behavior quite well, and even the threshold value of the 2D isomorphism coefficient calculated for the model systems also agrees perfectly with the experimental observations.

However, in the presence of a nanographene template, an increased tendency of mixing is revealed: the distribution of n_t indicates that partial mixing occurs for combinations with a 2D isomorphism coefficient as low as 0.42. Phase separation only becomes complete for the maximum difference in alkoxy chain length investigated, that is, for DBA-OC_{10}/DBA-OC_{20}, which has a negative 2D isomorphism coefficient due to the large difference in unit cell parameters. Due to the weak nature of the van der Waals interactions between interdigitated alkoxy chains, a slight mismatch because of a small difference in alkoxy chain length (*e.g.*, $OC_{14}H_{29}$ *versus* $OC_{16}H_{33}$) does not lead to a significant difference in the system's free energy. Nanographenes stabilize the nanowells, and their templating effect (*i.e.*, the formation of a porous pattern under concentration conditions where in the absence of nanographenes a high-density phase would be formed) overrules the self-recognition at the level of the alkoxy chains, leading to a significant mixing of the DBA molecules.

Though one may argue that this "*template inclusion induced transformation*" is kinetic in nature, experiments at DBA concentrations where porous honeycomb networks intrinsically prevail do not show any significant difference in phase behavior in the presence of nanographene guests, demonstrating that the increased tendency of mixing in the presence of nanographene is a thermodynamic effect.

These results could be helpful for the understanding of phase behavior of complex assembling systems at the solid–liquid interface and pave the way for the programmed fabrication of complex functional assemblies.

EXPERIMENTAL SECTION

Stock solutions of DBAs with a weight concentration of 1 mg/g in 1,2,4-trichlorobenzene (TCB) were used to prepare binary mixtures (normally 1:1, in volume) of DBAs with different alkoxy chains. The exact mole concentrations are mentioned in the figure captions. TCB was chosen because these DBA derivatives are very soluble, and more importantly, this solvent favors the formation of porous networks. Also important is that the assembling behavior of these molecules has been well-investigated at the TCB/graphite interface.[27–31] For investigations on the effect of template or guest accommodation, the original binary solutions were mixed with a saturated nanographene solution in TCB (0.034 mg/g) at a 1:1 volume ratio and then diluted until 0.05 mg/g at the level of the DBAs (in total). The exact concentrations of the species are indicated in the figure captions.

For STM measurements, a drop of one of the above solutions was applied on a freshly cleaved graphite substrate (HOPG, grade ZYB, Advanced Ceramics Inc., Cleveland, OH). STM images were acquired either using a PicoSPM (Agilent) or Nanoscope IIID (Veeco Instruments) operating in the constant current mode with the tip immersed in the solution at room temperature (21–22 °C). Pt/Ir (80%/20%) tips were prepared by mechanical cutting. The graphite lattice was recorded by lowering the bias right after obtaining images of the assembly. The drift of the image was corrected using the scanning probe image processor (SPIP) software (Image Metrology ApS) against the graphite lattice.

For a statistical evaluation of the distribution of template or guest molecules per cavity (n_t), for each sample, at least 15 to 20 medium-scale images (50 nm × 50 nm or 60 nm × 60 nm) were collected at different sites. Images were also collected in several sessions. Medium-scale rather than large-scale (120 nm × 120 nm) images were used because it is easier to identify the number of templates or guests per cavity unambiguously.

Since the STM measurements were conducted with an open sample holder, solvent evaporation is inevitable, and the DBA concentration must increase in time. To evaluate the effect of solvent evaporation quantitatively, we have carried out a control experiment where we monitored the evaporation of a droplet of the TCB solvent (about 8 to 9 μL) deposited on the surface of a freshly cleaved piece of HOPG (the same size as used for STM measurements) at 21 °C. During a typical STM session which lasts 30 to 40 min, 15% of the solvent evaporated. Therefore, solvent evaporation leads to a maximum increase in DBA concentration of about 18%. This change has a negligible impact on our data treatment as the concentration intervals are much larger.

Acknowledgment. This work is supported by the Fund of Scientific Research–Flanders (FWO), K.U. Leuven (GOA), the Belgian Federal Science Policy Office through IAP-6/27, Grant-in-Aid for Scientific Research from the Ministry of Education, Culture, Sports, Science, and Technology, Japan, JSPS and FWO under the Japan–Belgium Research Cooperative Program, and the start-up funding of HIT, New Century Excellent Talents in University (NCET) from the Ministry of Education of P. R. China and the fundamental research funds for the central universities HIT.BRET2.2010002.

Supporting Information Available: Extra STM and Monte Carlo simulation results, method for the calculation of l_{2Dt}, and rescaling of the system size. This material is available free of charge *via* the Internet at http://pubs.acs.org.

REFERENCES AND NOTES

1. Cicoira, F.; Santato, C.; Rosei, F. Two-Dimensional Nanotemplates as Surface Cues for the Controlled Assembly of Organic Molecules. *Top. Curr. Chem.* **2008**, *285*, 203–267.

2. Furukawa, S.; De Feyter, S. Two-Dimensional Crystal Engineering at the Liquid–Solid Interface. *Top. Curr. Chem.* **2009**, *287*, 87–133.
3. Piot, L.; Bonifazi, D.; Samori, P. Organic Reactivity in Confined Spaces under Scanning Tunneling Microscopy Control: Tailoring the Nanoscale World. *Adv. Funct. Mater.* **2007**, *17*, 3689–3693.
4. Hietschold, M.; Lackinger, M.; Griessl, S.; Heckl, W. M.; Gopakumar, T. G.; Flynn, G. W. Molecular Structures on Crystalline Metallic Surfaces: From STM Images to Molecular Electronics. *Microelectron. Eng.* **2005**, *82*, 207–214.
5. Mena-Osteritz, E.; Bäuerle, P. Complexation of C-60 on a Cyclothiophene Monolayer Template. *Adv. Mater.* **2006**, *18*, 447–451.
6. Merz, L.; Güntherodt, H. J.; Scherer, L. J.; Constable, E. C.; Housecroft, C. E.; Neuberger, M.; Hermann, B. A. Octyl-Decorated Frechet-Type Dendrons: A General Motif for Visualisation of Static and Dynamic Behaviour Using Scanning Tunnelling Microscopy. *Chem.—Eur. J.* **2005**, *11*, 2307–2318.
7. Zhang, J.; Li, B.; Cui, X.; Wang, B.; Yang, J.; Hou, J. G. Spontaneous Chiral Resolution in Supramolecular Assembly of 2,4,6-Tris(2-pyridyl)-1,3,5-triazine on Au(111). *J. Am. Chem. Soc.* **2009**, *131*, 5885–5890.
8. Plass, K. E.; Grzesiak, A. L.; Matzger, A. J. Molecular Packing and Symmetry of Two-Dimensional Crystals. *Acc. Chem. Res.* **2007**, *40*, 287–293.
9. Yoshimoto, S.; Higa, N.; Itaya, K. Two-Dimensional Supramolecular Organization of Copper Octaethylporphyrin and Cobalt Phthalocyanine on Au(III): Molecular Assembly Control at an Electrochemical Interface. *J. Am. Chem. Soc.* **2004**, *126*, 8540–8545.
10. Yang, X.; Mu, Z.; Wang, Z.; Zhang, X.; Wang, J.; Wang, Y. STM Study on Quinacridone Derivative Assemblies: Modulation of the Two-Dimensional Structure by Coadsorption with Dicarboxylic Acids. *Langmuir* **2005**, *21*, 7225–7229.
11. Huang, Y. L.; Chen, W.; Li, H.; Ma, J.; Pflaum, J.; Wee, A. T. S. Tunable Two-Dimensional Binary Molecular Networks. *Small* **2010**, *6*, 70–75.
12. Zhong, D.; Wedeking, K.; Blömker, T.; Erker, G.; Fuchs, H.; Chi, L. Multilevel Supramolecular Architectures Self-Assembled on Metal Surfaces. *ACS Nano* **2010**, *4*, 1997–2002.
13. Kudernac, T.; Lei, S.; Elemans, J. A. A. W.; De Feyter, S. Two-Dimensional Supramolecular Self-Assembly: Nanoporous Networks on Surfaces. *Chem. Soc. Rev.* **2009**, *38*, 402–421.
14. Stepanow, S.; Lin, N.; Barth, J. V.; Kern, K. Non-covalent Binding of Fullerenes and Biomolecules at Surface-Supported Metallosupramolecular Receptors. *Chem. Commun.* **2006**, 2153–2155.
15. Griessl, S. J. H.; Lackinger, M.; Jamitzky, F.; Markert, T.; Hietschold, M.; Heckl, W. M. Incorporation and Manipulation of Coronene in an Organic Template Structure. *Langmuir* **2004**, *20*, 9403–9407.
16. Lu, J.; Lei, S. B.; Zeng, Q. D.; Kang, S. Z.; Wang, C.; Wan, L. J.; Bai, C. L. Template-Induced Inclusion Structures with Copper(II) Phthalocyanine and Coronene as Guests in Two-Dimensional Hydrogen-Bonded Host Networks. *J. Phys. Chem. B* **2004**, *108*, 5161–5165.
17. Wahl, M.; Stöhr, M.; Spillmann, H.; Jung, T. A.; Gade, L. H. Rotation–Libration in a Hierarchic Supramolecular Rotor–Stator System: Arrhenius Activation and Retardation by Local Interaction. *Chem. Commun.* **2007**, 1349–1351.
18. Gimzewski, J. K.; Joachim, C.; Schlittler, R. R.; Langlais, V.; Tang, H.; Johannsen, I. Rotation of a Single Molecule within a Supramolecular Bearing. *Science* **1998**, *281*, 531–533.
19. Macleod, J. M.; Ivasenko, O.; Fu, C.; Taerum, T.; Rosei, F.; Perepichka, D. F. Supramolecular Ordering in Oligothiophene–Fullerene Monolayers. *J. Am. Chem. Soc.* **2009**, *131*, 16844–16850.
20. Schlickum, U.; Decker, R.; Klappenberger, F.; Zoppellaro, G.; Klyatskaya, S.; Ruben, M.; Silanes, I.; Arnau, A.; Kern, K.; Brune, H.; Barth, J. V. Metal–Organic Honeycomb Nanomeshes with Tunable Cavity Size. *Nano Lett.* **2007**, *7*, 3813–3817.
21. Lei, S.; Tahara, K.; Adisoejoso, J.; Balandina, T.; Tobe, Y.; De Feyter, S. Towards Two-Dimensional Nanoporous Networks: Crystal Engineering at the Solid–Liquid Interface. *CrystEngComm* **2010**, *12*, 3369–3381.
22. Kampschulte, L.; Werblowsky, T. L.; Kishore, R. S. K.; Schmittel, M.; Heckl, W. M.; Lackinger, M. Thermodynamical Equilibrium of Binary Supramolecular Networks at the Liquid–Solid Interface. *J. Am. Chem. Soc.* **2008**, *130*, 8502–8507.
23. N. Wintjes, N.; Hornung, J.; Lobo-Checa, J.; Voigt, T.; Samuely, T.; Thilgen, C.; Stöhr, M.; Diederich, F.; Jung, T. A. Supramolecular Synthons on Surfaces: Controlling Dimensionality and Periodicity of Tetraarylporphyrin Assemblies by the Interplay of Cyano and Alkoxy Substituents. *Chem.—Eur. J.* **2008**, *14*, 5794–5802.
24. Stepanow, S.; Lin, N.; Payer, D.; Schlickum, U.; Klappenberger, F.; Zoppellaro, G.; Ruben, M.; Brune, H.; Barth, J. V.; Kern, K. Surface-Assisted Assembly of 2D Metal–Organic Networks That Exhibit Unusual Threefold Coordination Symmetry. *Angew. Chem., Int. Ed.* **2007**, *46*, 710–713.
25. Stepanow, S.; Lingenfelder, M.; Dmitriev, A.; Spillmann, H.; Delvigne, E.; Lin, N.; Deng, X.; Cai, C.; Barth, J. V.; Kern, K. Steering Molecular Organization and Host–Guest Interactions Using Two-Dimensional Nanoporous Coordination Systems. *Nat. Mater.* **2004**, *3*, 229–233.
26. Perdigão, L. M. A.; Saywell, A.; Fontes, G. N.; Staniec, P. A.; Goretzki, G.; Phillips, A. G.; Champness, N. R.; Beton, P. H. Functionalized Supramolecular Nanoporous Arrays for Surface Templating. *Chem.—Eur. J.* **2008**, *14*, 7600–7607.
27. Tahara, K.; Furukawa, S.; Uji-i, H.; Uchino, T.; Ichikawa, T.; Zhang, J.; Mamdouh, W.; Sonoda, M.; De Schryver, F. C.; De Feyter, S.; *et al.* Two-Dimensional Porous Molecular Networks of Dehydrobenzo[12]annulene Derivatives *via* Alkyl Chain Interdigitation. *J. Am. Chem. Soc.* **2006**, *128*, 16613–16625.
28. Furukawa, S.; Uji-i, H.; Tahara, K.; Ichikawa, T.; Sonoda, M.; De Schryver, F. C.; Tobe, Y.; De Feyter, S. Molecular Geometry Directed Kagome and Honeycomb Networks: Toward Two-Dimensional Crystal Engineering. *J. Am. Chem. Soc.* **2006**, *128*, 3502–3503.
29. Tahara, K.; Lei, S.; Adisoejoso, J.; De Feyter, S.; Tobe, Y. Supramolecular Surface-Confined Architectures Created by Self-Assembly of Triangular Phenylene–Ethynylene Macrocycles *via* van der Waals Interaction. *Chem. Commun.* **2010**, 8507–8525.
30. Furukawa, S.; Tahara, K.; De Schryver, F. C.; Van der Auweraer, M.; Tobe, Y.; De Feyter, S. Structural Transformation of a Two-Dimensional Molecular Network in Response to Selective Guest Inclusion. *Angew. Chem., Int. Ed.* **2007**, *46*, 2831–2834.
31. Lei, S.; Tahara, K.; Feng, X.; Furukawa, S.; De Schryver, F. C.; Müllen, K.; Tobe, Y.; De Feyter, S. Molecular Clusters in Two-Dimensional Surface-Confined Nanoporous Molecular Networks: Structure, Rigidity, and Dynamics. *J. Am. Chem. Soc.* **2008**, *130*, 7119–7129.
32. Theobald, J. A.; Oxtoby, N. S.; Philips, M. A.; Champness, N. R.; Beton, P. H. Controlling Molecular Deposition and Layer Structure with Supramolecular Surface Assemblies. *Nature* **2003**, *424*, 1029–1031.
33. Langner, A.; Tait, S. L.; Lin, N.; Rajadurai, C.; Ruben, M.; Kern, K. Self-Recognition and Self-Selection in Multicomponent Supramolecular Coordination Networks on Surfaces. *Proc. Natl. Acad. Sci. U.S.A.* **2007**, *104*, 17927–17930.
34. Schull, G.; Douillard, L.; Fiorini-Debuisschert, C.; Charra, F.; Mathevet, F.; Kreher, D.; Attias, A. Selectivity of Single-Molecule Dynamics in 2D Molecular Sieves. *Adv. Mater.* **2006**, *18*, 2954–2957.
35. Lei, S.; Surin, M.; Tahara, K.; Adisoejoso, J.; Lazzaroni, R.; Tobe, Y.; De Feyter, S. Programmable Hierarchical Three-Component 2D Assembly at a Liquid–Solid Interface: Recognition, Selection, and Transformation. *Nano Lett.* **2008**, *8*, 2541–2546.
36. Llanes-Pallas, A.; Palma, C. A.; Piot, L.; Belbakra, A.; Listorti, A.; Prato, M.; Samor, P.; Armaroli, N.; Bonifazi, D. Engineering of Supramolecular H-Bonded Nanopolygons

via Self-Assembly of Programmed Molecular Modules. *J. Am. Chem. Soc.* **2009**, *131*, 509–520.
37. Li, Y.; Ma, Z.; Deng, K.; Lei, S.; Zeng, Q.; Fan, X.; De Feyter, S.; Huang, W.; Wang, C. Thermodynamic Controlled Hierarchical Assembly of Ternary Supramolecular Networks at the Liquid−Solid Interface. *Chem.—Eur. J.* **2009**, *15*, 5418–5423.
38. Ciesielski, A.; Palma, C. A.; Bonini, M.; Samor, P. Towards Supramolecular Engineering of Functional Nanomaterials: Pre-programming Multi-component 2D Self-Assembly at Solid−Liquid Interfaces. *Adv. Mater.* **2010**, *22*, 3506–3520.
39. Bonifazi, D.; Mohnani, S.; Llanes-Pallas, A. Supramolecular Chemistry at Interfaces: Molecular Recognition on Nanopatterned Porous Surfaces. *Chem.—Eur. J.* **2009**, *15*, 7004–7025.
40. Inaba, A.; Clarke, S. M.; Arnold, T.; Thomas, R. K. Mixing Behaviour in 2D Layers of Linear Alkanes Adsorbed on Graphite. *Chem. Phys. Lett.* **2002**, *352*, 57–62.
41. Messe, L.; Clarke, S. M.; Dong, C.; Thomas, R. K.; Inaba, A.; Alba, M. D.; Castro, M. A. Mixing Behavior at the Solid/Liquid Interface: Binary Alcohol Monolayers on Graphite. *Langmuir* **2002**, *18*, 9429–9433.
42. Messe, L.; Perdigon, A.; Clarke, S. M.; Inaba, A.; Arnold, T. Alkane/Alcohol Mixed Monolayers at the Solid/Liquid Interface. *Langmuir* **2005**, *21*, 5085–5093.
43. The 2D isomorphism coefficient, I_{2D}, is defined as $I_{2D} = 1 - A_{un}/A_{com}$, where A_{un} and A_{com} are the areas uncommon and common for both unit cells of the two species.
44. Wintjes, N.; Bonifazi, D.; Cheng, F.; Kiebele, A.; Stöhr, M.; Jung, T.; Spillmann, H.; Diederich, F. A Supramolecular Multiposition Rotary Device. *Angew. Chem., Int. Ed.* **2007**, *46*, 4089–4092.
45. Silien, C.; Räisänen, M. T.; Buck, M. A Supramolecular Hydrogen-Bonded Network as a Diffusion Barrier for Metal Adatoms. *Angew. Chem., Int. Ed.* **2009**, *48*, 3349–3352.
46. Li, S. S.; Yan, H. J.; Wan, L. J.; Yang, H. B.; Northrop, B. H.; Stang, P. J. Control of Supramolecular Rectangle Self-Assembly with a Molecular Template. *J. Am. Chem. Soc.* **2007**, *129*, 9268–9269.
47. Madueno, R.; Räisänen, M. T.; Silien, C.; Buck, M. Functionalizing Hydrogen-Bonded Surface Networks with Self-Assembled Monolayers. *Nature* **2008**, *454*, 618–621.
48. Linares, M.; Minoia, A.; Brocorens, P.; Beljonne, D.; Lazzaroni, R. Expression of Chirality in Molecular Layers at Surfaces: Insights from Modelling. *Chem. Soc. Rev.* **2009**, *38*, 806–816.
49. Blunt, M.; Lin, X.; Gimenez-Lopez, M.; Schröder, M.; Champness, N. R.; Beton, P. H. Directing Two-Dimensional Molecular Crystallization Using Guest Templates. *Chem. Commun.* **2008**, *20*, 2304–2306.
50. Palma, C. A.; Bjork, J.; Bonini, M.; Dyer, M. S.; Llanes-Pallas, A.; Bonifazi, D.; Persson, M.; Samor, P. Tailoring Bicomponent Supramolecular Nanoporous Networks: Phase Segregation, Polymorphism, and Glasses at the Solid−Liquid Interface. *J. Am. Chem. Soc.* **2009**, *131*, 13062–13071.
51. Otero, R.; Xu, W.; Lukas, M.; Kelly, R. E. A.; Lægsgaard, E.; Stensgaard, I.; Kjems, J.; Kantorovich, L. N.; Besenbacher, F. Specificity of Watson−Crick Base Pairing on a Solid Surface Studied at the Atomic Scale. *Angew. Chem., Int. Ed.* **2008**, *47*, 9673–9676.
52. Ma, X. J.; Yang, Y. L.; Deng, K.; Zeng, Q. D.; Wang, C.; Zhao, K. Q.; Hu, P.; Wang, B. Q. Identification of a Peripheral Substitution Symmetry Effect in Self-Assembled Architectures. *ChemPhysChem* **2007**, *8*, 2615–2620.
53. Seitsonen, A. P.; Lingenfelder, M.; Spillmann, H.; Dmitriev, A.; Stepanow, S.; Lin, N.; Kern, K.; Barth, J. V. Density Functional Theory Analysis of Carboxylate-Bridged Diiron Units in Two-Dimensional Metal−Organic Grids. *J. Am. Chem. Soc.* **2006**, *128*, 5634–5635.
54. Weber, U. K.; Burlakov, V. M.; Perdigão, L. M. A.; Fawcett, R. H. J.; Beton, P. H.; Champness, N. R.; Jefferson, J. H.; Briggs, G. A. D.; Pettifor, D. G. Role of Interaction Anisotropy in the Formation and Stability of Molecular Templates. *Phys. Rev. Lett.* **2008**, *100*, 156101.
55. Szabelski, P.; De Feyter, S.; Drach, M.; Lei, S. Computer Simulation of Chiral Nanoporous Networks on Solid Surfaces. *Langmuir* **2010**, *26*, 9506–9515.
56. Normally when using molecular dynamics to model the self-assembly, an initial ordered structure has to be assumed. In contrast in the MC method, we can start from total randomness and let the molecules self-organize into some pattern which they chose to be optimal instead of guess and assume any initial pattern to check its stability.
57. Szabelski, P. Extended Surface Chirality for Enantiospecific Adsorption. *Chem.—Eur. J.* **2008**, *14*, 8312–8321.
58. Silly, F.; Weber, U. K.; Shaw, A. Q.; Burlakov, V. M.; Castell, M. R.; Briggs, G. A. D.; Pettifor, D. G. Deriving Molecular Bonding from a Macromolecular Self-Assembly Using Kinetic Monte Carlo Simulations. *Phys. Rev. B* **2008**, *77*, 201408(R).
59. Garrahan, J. P.; Stannard, A.; Blunt, M. O.; Beton, P. H. Molecular Random Tilings as Glasses. *Proc. Natl. Acad. Sci. U.S.A.* **2009**, *106*, 15209–15213.
60. Blunt, M. O.; Russell, J. C.; Giménez-López, M.; Garrahan, J. P.; Lin, X.; Schröder, M.; Champness, N. R.; Beton, P. H. Random Tiling and Topological Defects in a Two-Dimensional Molecular Network. *Science* **2008**, *322*, 1077–1081.
61. Lei, S.; Tahara, K.; De Schryver, F. C.; Van der Auweraer, M.; Tobe, Y.; De Feyter, S. One Building Block, Two Different Supramolecular Surface-Confined Patterns: Concentration in Control at the Solid−Liquid Interface. *Angew. Chem., Int. Ed.* **2008**, *47*, 2964–2968.
62. Lei, S.; Tahara, K.; Tobe, Y.; De Feyter, S. Role of Pseudopolymorphism on Concentration Dependent Competitive Adsorption at a Liquid/Solid Interface. *Chem. Commun.* **2010**, *46*, 9125–9127.
63. Note, for different DBAs, this concentration is different.
64. Clarke, S. M.; Messe, L.; Adams, J.; Inaba, A.; Arnold, T.; Thomas, R. K. A Quantitative Parameter for Predicting Mixing Behaviour in Adsorbed Layers: The 2D Isomorphism Coefficient. *Chem. Phys. Lett.* **2003**, *373*, 480–485.
65. Rajabalee, F.; Espeau, P.; Haget, Y. *n*-Octane Plus *n*-Decane: A Eutectic System in the *n*-Alkane Family; Experimental Phase Diagram and Thermodynamic Analysis. *Mol. Cryst. Liq. Cryst. Sci. Technol., Sect. A* **1995**, *269*, 165–173.
66. Mondieig, D.; Rajabalee, F.; Metivaud, V.; Oonk, H. A. J.; Cuevas-Diarte, M. A. *n*-Alkane Binary Molecular Alloys. *Chem. Mater.* **2004**, *16*, 786–798.
67. Hoffmann, H.; Pössnecker, G. The Mixing Behavior of Surfactants. *Langmuir* **1994**, *10*, 381–389.
68. De Vries, A. H.; Mark, A. E.; Marrink, S. J. The Binary Mixing of Phospholipids in a Bilayer: A Molecular Dynamics Study. *J. Phys. Chem. B* **2004**, *108*, 2454–2463.
69. Frenkel, D.; Smit, B. *Understanding Molecular Simulation*; Academic Press: London, 2002.
70. The distribution expected from complete phase separation without preferential adsorption is obtained by averaging the abundance of clusters in DBA-OC_{16} and DBA-OC_{20}.
71. Castro, M. A.; Clarke, S. M.; Inaba, A.; Thomas, R. K.; Arnold, T. Preferential Adsorption from Binary Mixtures of Short Chain *n*-Alkanes: The Octane-Decane System. *J. Phys. Chem. B* **2001**, *105*, 8577–8582.
72. In statistics in Figure 14c, the pores with unidentified number of guests were not taken into account. This makes it easier to compare the influence of concentration on the distribution of n_t. A similar histogram, but with the pores with unidentified number of guests also taken into account, is shown in Figure S5 in Supporting Information.
73. Kim, K.; Plass, K. E.; Matzger, A. J. Kinetic and Thermodynamic Forms of a Two-Dimensional Crystal. *Langmuir* **2003**, *19*, 7149–7152.